International Journal of Heat and Fluid Flow 30 (2009) 1007–1015

Contents lists available at ScienceDirect

International Journal of Heat and Fluid Flow

journal homepage: www.elsevier.com/locate/ijhff

Turbulent channel flow with 2D wedges of random height on one wall

Jorge Bailon-Cuba [a], Stefano Leonardi [b,*], Luciano Castillo [c]

[a] Technical University of Ilmenau, 98693 Ilmenau, Germany
[b] University of Puerto Rico at Mayaguez, Department of Mechanical Engineering, Mayaguez, PR 00680, Puerto Rico
[c] Rensselaer Polytechnic Institute, Department of Mechanical Engineering, Aeronautical and Mechanics, Troy, NY 12180, United States

ARTICLE INFO

Article history:
Received 16 May 2008
Received in revised form 12 March 2009
Accepted 31 March 2009
Available online 15 May 2009

Keywords:
Roughness
Random
Turbulence
DNS

ABSTRACT

Direct numerical simulations (DNS) of a turbulent channel flow with 2D wedges of random height on the bottom wall have been performed. In addition, two other simulations have been carried out to assess the effect of the geometry on the overlying flow. In the first simulation, the four smallest elements were removed while in the other, a uniform distribution of wedges with the same area was used. Two Reynolds numbers were studied, $Re_b = 2500$ and $Re_b = 5000$ which correspond in case of smooth walls to $Re_\tau = 180$ and 300, respectively. Roughness on the wall induces separated regions, the reattachment occurring on the walls of the wedges or on the bottom wall. The pressure gradients on the walls increase the ejections and inrushes towards the wall. As a consequence the flow is more isotropic. The mechanism inducing an improved isotropy has been explained in term of the spectra and budgets of Reynolds stress. The comparison of the 3 surfaces has shown that near the wall, the uniformly distributed roughness represents only a poor approximation of the surface with wedges of random height. The Reynolds stresses, pressure distribution and spectra on the modified wall agree well with those on the random surface. Energy spectra show the pitch to height ratio of the largest elements to be the more appropriate geometrical parameter to describe the geometry.

© 2009 Elsevier Inc. All rights reserved.

1. Introduction

Roughness plays a key role in many industrial applications including flows in pipelines as oil and gas. In addition, roughness becomes important in high Reynolds number flows. Many studies have attempted to quantify the effect of roughness on the overlying flow. According to the classical literature (i.e. Nikuradse (1933), Clauser (1954), Rotta (1962), Perry et al. (1969)), the effect of the roughness is to shift the mean velocity profile, scaled in wall units, downward with respect to that on a smooth wall:

$$U^+ = \kappa^{-1} \ln y^+ + C - \Delta U^+ \quad (1)$$

where C and κ are constants and "+" denotes normalization by wall variables U_τ ($\equiv \sqrt{\tau_w/\rho}$, where τ_w is the wall shear stress equal to the sum of the viscous (or skin frictional) drag and the form drag) and ν/U_τ. The roughness function, ΔU^+, contains the effect of roughness and depends on the density (defined as the total roughness frontal area per unit wall area), height (k) and nature of the roughness.

Most of the research on rough walls relies on 2D or 3D deterministic roughness (square bars, Perry et al. (1969), Leonardi et al. (2003), Krogstad et al. (2005), Ikeda and Durbin (2007)). However the roughness encountered in nature is random, i.e. the roughness height and pitch to height values vary randomly. Many experiments have been performed using sand grain roughness as a model of random roughness, from the pioneering work of Nikuradse (1933), to the recent contribution of McKeon et al. (2004), Flack et al. (2005), Schultz and Flack (2005) and Brzek et al. (2007, 2008). Schlichting (1960) was critical in the use of sand grain roughness since it was difficult to be reproduced and quantified. Shockling et al. (2006) studied honed pipe and introduced the high spot count wavelength, λ_{HSC}, as an estimate of the typical distance between the large roughness elements, to characterize random roughness. In fact, the distance between the higher roughness elements must be an important parameter to characterize the flow since small roughness elements should not play an important role when shielded by the larger elements.

A systematic study of random roughness was carried out by Cheng and Castro (2002). They used x-wire anemometry in a wind tunnel to measure the flow over a number of urban-blocks all having 25% plan and frontal area density. Comparisons were made between a homogeneous (regular element array) surface and one consisting of random height elements of the same total volume. Aligned and staggered patterns of rectangular prisms were considered as roughness elements. Staggered cube arrays provided greater drag than the aligned cube arrays. In addition, it was demonstrated that random height roughness of the same plan

* Corresponding author.
E-mail address: sleonardi@me.uprm.edu (S. Leonardi).

0142-727X/$ - see front matter © 2009 Elsevier Inc. All rights reserved.
doi:10.1016/j.ijheatfluidflow.2009.03.017

arrangement and total volume as a regular array produced higher shear stress.

A first attempt to consider numerically roughness elements of different height was carried out by Ikeda and Durbin (2007). They performed a DNS of turbulent flow over rectangular ribs transversely mounted on one wall of a a channel, the other being smooth. The ribs are widely separated with $\lambda/k = 9$, (λ being the pitch, k the height of the roughness elements). To mimic random roughness, another case with two rib-heights was considered. Unevenness was imposed by alternatively increasing and decreasing the original square rib height by 15%. For the uneven case, a shorter recirculation region for the smaller rib provides a longer distance to form a fully rough velocity profile. This increases the mass flux upstream of the taller rib within the roughness sublayer, and explains why the pressure drag acting on a taller rib is about 42% larger than that on a square rib (even case), with only a 15% increase in rib height.

The present paper further corroborate previous studies by clarifying how 2D roughness elements with random height affects the overlying flow. This has been investigated by performing a Direct Numerical Simulation of the flow in a channel with a lower wall made of 10 wedges of constant base and random height (hereafter random). Using a random number generator 10 numbers were obtained and scaled so as to have a maximum height of $k = 0.2h$ and a minimum height of $k = 0$. Two other simulations have been carried out as reference cases, one removing the four smallest elements of the random surface (hereafter modified), the other with a uniform distribution of wedges (hereafter uniform) of equivalent total area. The database here obtained allows us to assess if a generic random roughness can be represented more simply by the larger elements or by the average roughness density. The results have practical applications when modeling large areas of rough surfaces, where it is worth reducing the number of parameters necessary to describe the surface.

2. Numerical procedure

The incompressible non-dimensional Navier–Stokes and continuity Eqs. may be written as,

$$\frac{\partial u_i}{\partial t} + \frac{\partial u_i u_j}{\partial x_j} = -\frac{\partial P}{\partial x_i} + \frac{1}{Re}\frac{\partial^2 u_i}{\partial x_j^2} + \Pi\delta_{i1}, \quad \nabla\cdot\mathbf{u} = 0, \tag{2}$$

where Π is the pressure gradient required to maintain a constant flow rate; u_i, the component of the velocity vector in the $i-$direction and P the pressure. All the quantities have been normalized by a combination of the centerline velocity, U_c, and one half of channel's height, h. The Navier–Stokes equations have been discretized in an orthogonal coordinate system using the staggered central second-order finite difference approximation. Here we recall only the main features since details of the numerical method can be found in Orlandi (2000). The discretized system is advanced in time using a fractional-step method with viscous terms treated implicitly and convective terms explicitly. The large sparse matrix resulting from the implicit terms is inverted by an approximate factorization technique. At each time step, the momentum equations are advanced with the pressure at the previous step, yielding an intermediate non-solenoidal velocity field. A scalar quantity Φ projects the non-solenoidal field onto a solenoidal one. A hybrid low-storage third-order Runge–Kutta scheme is used to advance the equations in time.

The roughness is treated by the immersed boundary technique described in detail by Fadlun et al. (2000). This approach allows the solution of flows over complex geometries without the need of computational intensive body-fitted grids. It consists of imposing $U_i = 0$ on the body surface, which does not necessarily coincide with the grid (• in Fig. 1). The terms in the Navier–Stokes equations, at the first point outside the body, are discretized taking into account the real distance between the grid and the body (Orlandi and Leonardi, 2006). This is to avoid the roughness being described in a stepwise way. Periodic boundary conditions apply in the streamwise and spanwise directions, as well as a non-slip condition at the wall in the normal direction. In addition, the flow rate has been kept constant in all simulations. the computational box is $6h \times 2h \times \pi$ in x–y–z, respectively.

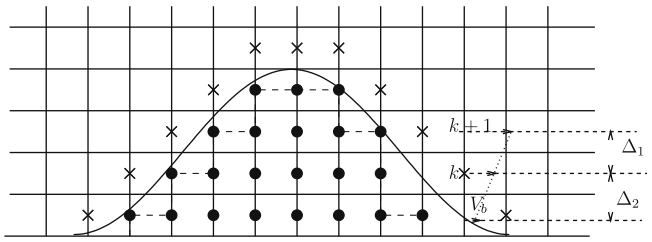

Fig. 1. Geometrical sketch of immersed boundary method. • points inside the roughness element; × points nearest to the boundary of the roughness element. A partial wavy wall is shown (—-).

The simulation is started from an initial condition imposing a Poiseuille mean velocity profile plus a random disturbance in the streamwise direction (x). A uniform coarse grid is used during the transient period, after which velocities are interpolated on a finer grid. The process is repeated until the results are grid independent. In Fig. 2 the mean and rms of streamwise velocity for random roughness are shown for three different grids: □ $96 \times 160 \times 300$, ○ $192 \times 160 \times 300$, — $192 \times 160 \times 600$. Averages are performed in time and in the spanwise direction. The mean velocity profiles relative to the 3 grids overlap closely. Larger variation are observed for the rms of streamwise velocity. Since the difference between the grid $192 \times 160 \times 300$ and finest grid, $193 \times 161 \times 601$, are small, the latter was used for all the simulations. For each case, two Reynolds numbers have been considered: $Re = \frac{Uh}{\nu} = 4,200$ and $7,000$ where U is the maximum velocity and correspond to $Re_b = 2500$ and $Re_b = 5000$ when the bulk velocity is used as reference velocity. The equivalent turbulent Reynolds number is $Re_\tau = \frac{U_\tau h}{\nu} = 180$ (as in Kim et al., 1987) and 300 when both walls are smooth.

3. Mean flow

Mean streamlines averaged in time and spanwise direction are shown in Fig. 3. At the upper vertex of the wedges a separation occurs. When the pitch to height ratio is small, $\lambda/k < 6$, reattachment is on the windward side of the following wedge. When the pitch to height ratio is large, $\lambda/k > 6$, reattachment occurs on the bottom wall. For example, the wedge 5 produces a separation, and the flow reattaches just upstream of wedge 7. The modified roughness surface (obtained by removing the 4 smallest elements) presents very similar streamlines. However, having removed wedge 7, the flow remains parallel to the bottom wall for a larger distance. Reattachment occurs at about $b/k_5 \approx 5$, where b is the horizontal distance measured from the separation point B and k_5 is the height of the fifth wedge (Fig. 3b). This agrees with results in literature. In fact, Le et al. (1997) performed a DNS of a turbulent flow over a backward facing step with inlet and outlet boundary conditions. They showed that the instantaneous reattachment location, averaged in z, oscillates between $X_r/k = 4.8$ and $X_r/k = 8$ (X_r is measured from the step) with an averaged value of about $6.3k$. Liu et al. (1966) reported a reattachment length of $6k$ for $w/k = 23$. For longitudinal square bars, Leonardi et al. (2003) found a reattachment length of $5.8k$. The

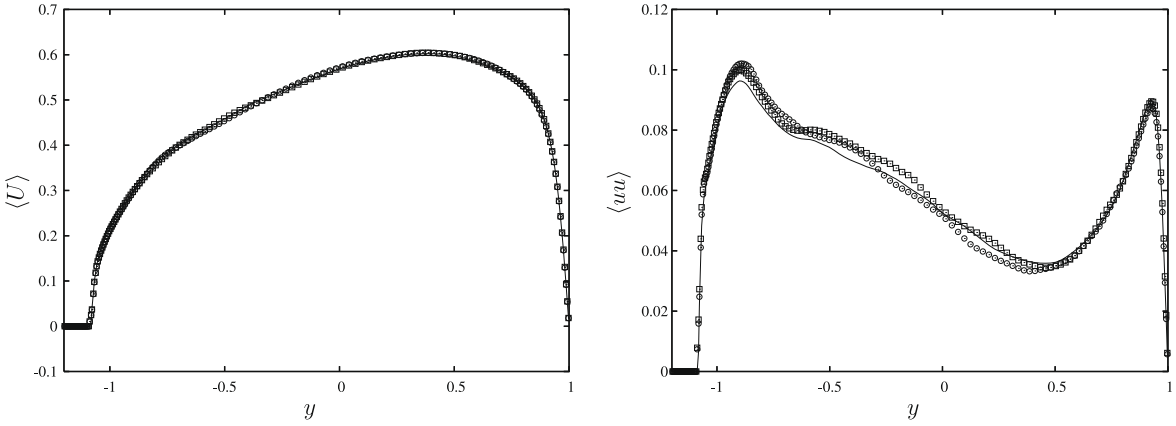

Fig. 2. Mean streamwise velocity (a) and streamwise velocity rms (b) for 3 different grids: □ $96 \times 160 \times 300$, ○ $192 \times 160 \times 300$, —- $192 \times 160 \times 600$.

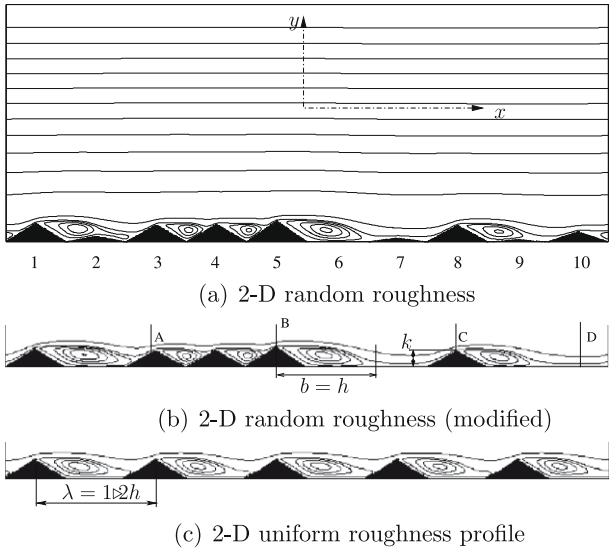

Fig. 3. Mean streamlines averaged in time, spanwise direction. From top to bottom: random roughness, modified random roughness, and uniform roughness. Wedges on the random roughness are labeled, the 6th having a height $k = 0$, the 5th $k = 0.2h$.

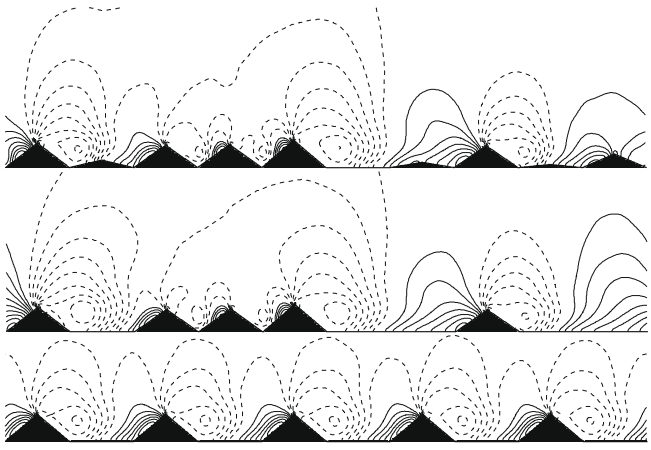

Fig. 4. Pressure fluctuation contours averaged in time and spanwise direction, increments $\Delta = 0.005$. Solid lines positive, dashed negative.

rough surface with a uniform distribution of wedges present a pitch to height ratio of 6.2. The width of the cavity on the bottom wall is $5.2k$ and it is too short to allow a reattachment on the bottom wall.

Pressure contours are shown in Fig. 4. The pressure has a peak in correspondence of the stagnation point on the windward side of the wedges. For the random and modified wall the pressure contours reach almost the centerline, whereas for the uniform roughness the disturbance remains limited to the near wall region. In fact, the higher peaks of pressure occur when the pitch to height ratio is larger, for example between wedge 1–3 and 5–8 of the random and modified surfaces. The difference between the highest and lowest values of pressure is $\Delta P = 0.127$, 0.117 and 0.103 for modified, random and uniform rough surfaces, respectively. This is due to the distribution of pitch to height ratio in the different surfaces. In fact, when the pitch to height ratio increases, the momentum of the flow within the roughness layer increases and so does ΔP. The λ/k value relative to the uniform distribution is the average of the λ/k relative to the random distribution. Therefore, in the random surface, some wedges have a larger λ/k and as a consequence a stronger ΔP. Near the wall, the pressure distribution of a uniform rough wall is a poor approximation of that over a random surface. The pressure distribution relative to the modified wall, compares well with that over the original-random wall.

The pressure distribution on the three rough walls is shown in Fig. 5a. In correspondence to the stagnation points, peaks of pressure are observed. Downstream of the stagnation point, a large favorable pressure gradient occurs. This produces an increase of velocity up to the crest of the element, where the flow separates due to the discontinuity in the geometry. For a large part at the beginning of the separated region the pressure is constant, and downstream it increases by approaching the stagnation point of the following element. The pressure distribution $P(x)$ on the frontal faces raises slightly when the smallest wedges are removed. However, $P(x)$ raises drastically when the removed wedge is a bit higher (i.e. 10th wedge). The slope of the adverse pressure gradient becomes lower and extends through larger distances. For the uniformly-spaced wedges, the pressure distribution is periodic with period $\lambda = 1.2h$ (the wedges spacing).

The projection in the streamwise direction of the pressure on the wall $\langle P \rangle \mathbf{n} \cdot \mathbf{x} \delta s$ represents the streamwise force exerted by pressure over the infinitesimal surface elements δs. The sum of these contributions, $P_d(x) = \int_0^x \langle P \rangle \mathbf{n} \cdot x \delta \mathbf{s}$, represents the form drag. In Fig. 5b, $P_d(x)$ is shown to understand which elements contribute more to the total drag. The maximum pressure drag corresponds to the uniformly-spaced profile. Leonardi et al. (2003) explained that the maximum drag occurs when $\lambda/k \approx 8$. The pitch to height value for the uniform case is $\lambda/k \approx 6$. On the other hand, the random roughness has a wide range of λ/k. For example, for

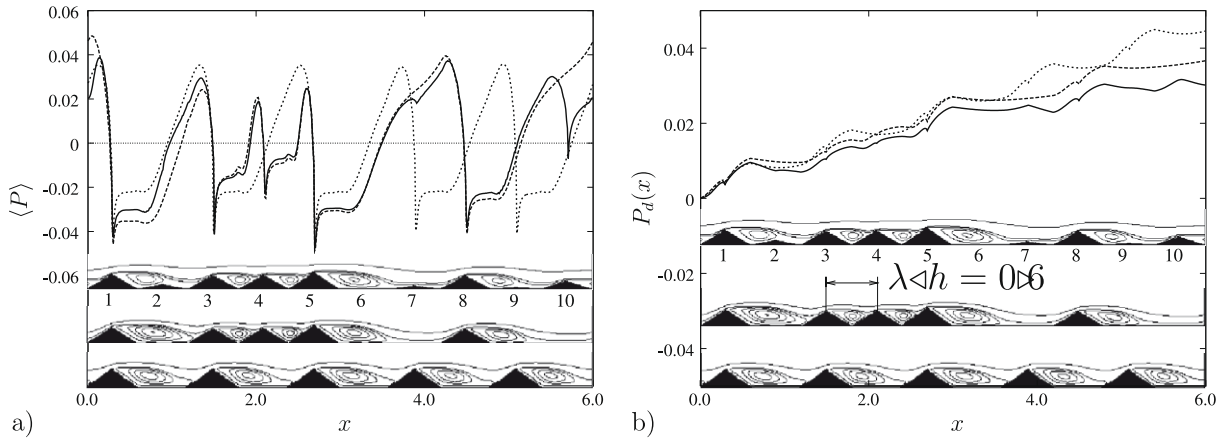

Fig. 5. (a) Pressure distribution (averaged in time and spanwise direction) on the rough walls: ——, random; - - - -, modified; ....., uniform. (b) Pressure drag projected in streamwise direction: ——, random; - - - -, modified; ....., uniform.

$1.5 < x < 3$, $\lambda/k = 3$, and the relative form drag is small. When the smallest elements are removed, the pitch to distance value increases and so does the form drag.

For the periodic profile, the high pressure gradient occurs periodically along the windward faces (except between the stagnation point and the peak) and back faces of the wedges. Also, the minimum pressure drag for the original-random geometry is due to the flow around the smallest wedges for which the acceleration between the stagnation points and their vertices is relatively small and the local drag at their back faces is negative (wedges 7, 9, and 10) or mostly negative (wedge 2).

4. Roughness function

Direct Numerical Simulations allow the friction velocity, U_τ, to be estimated reliably as $U_\tau = \sqrt{\tau_w}$ where $\tau_w = \sqrt{\overline{P_d} + \overline{C_f}}$ is the sum of the pressure and frictional drag, respectively (the overbar means averaging in x, z and time, $\overline{C_f} = \lambda^{-1} \int_0^\lambda \langle C_f \rangle ds$). An alternative method, described in detail by Leonardi et al. (2005) determines U_τ once the zero crossing of uv and the total pressure drop of the channel (Π) are known. Table 1 shows that the values of U_τ computed with both methods agree well. The table shows also the C_f/P_d ratio. The frictional drag is much lower than the pressure drag, the minimum C_f/P_d occurring for the wall with uniformly distributed wedges. In fact, being the frictional drag small, the minimum C_f/P_d corresponds to the wall with the maximum form drag (the wall with wedges uniformly spaced). Brzek et al. (2008) showed similar decomposition for a turbulent boundary layer in transitional regime and fully rough. The maximum U_τ corresponds to the uniform wedges because it has the higher pressure drag.

The effect of roughness on the overlying flow is usually quantified by the roughness function ΔU^+ (eq.1), the downward shift of the velocity profile in wall units with respect to the smooth wall.

Table 1
C_f/P_d ratio and values of U_τ calculated as the sum of the pressure and frictional drag and using the zero crossing of uv (h_1 and h_2 are the distances from the wall to y_{uv}).

Geometry	Random	Modified	Uniform
C_f/P_d ($\approx$)	0.477	0.382	0.273
$U_\tau = \sqrt{\tau}$	0.0738	0.0801	0.0869
$U_\tau = \sqrt{\frac{2\Pi h}{1+h_1/h_2}}$	0.0731	0.0785	0.0879
Uncertainty (%)	0.93	2.15	1.16

The velocity profiles in wall units are shown in Fig. 6a. The origin for y has been determined by matching the slopes in the log-law region with the value $1/0.41$. The shift in the origin in terms of the maximum roughness height $k = 0.2$ is about $\epsilon/k = 0.4$. The velocity profiles relative to random and modified rough walls almost overlap both at $Re_b = 2500$ and $Re_b = 5000$. The uniform rough surface exhibits the largest roughness function at both Reynolds numbers. The modified rough surface represents well the random rough wall while the wall with wedges uniformly spaced is only a poor approximation of the random geometry. Therefore, it is more accurate to model a random roughness by removing the smallest elements (filtering at a particular height) rather than using the equivalent average roughness density.

For a k-type surface, in the fully rough regime, ΔU^+ is a function of the roughness height scaled in wall units (Perry et al., 1969):

$$\Delta U^+ = \kappa^{-1} \ln k^+ + B. \tag{3}$$

Fig. 6b shows the roughness function as a function of the roughness height. Since two of the walls present non uniform roughness height, $\epsilon = 0.4k$ has been taken as the reference roughness height. All the points agree well with Eq. (3) denoting that the flow is in the fully rough regime.

5. Turbulence intensities and Reynolds stress

The roughness on the wall induces favorable and adverse pressure gradients in correspondence of stagnation and separation points. As a consequence, the ejections and inrushes towards the wall increase. The root mean square of streamwise (u_{rms}) and of wall normal velocity (v_{rms}) increase with respect to those over a flat wall. High levels of u_{rms} and v_{rms} are observed at the crest plane, at about the center of the cavities (Fig. 7). On the wall with wedges of random height (Fig. 7a), the cavities have several aspect ratios. When the pitch over height ratio is large, the u_{rms} and v_{rms} are larger than those over a small aspect ratio cavity. Waviness in the contours of u_{rms} and v_{rms} can be observed up to $y/h = -0.5$, about $5k$ over the crests plane. The rough wall acts as a perturbation on the overlying flow, and the penetration of such disturbances varies with the aspect ratio of the cavities. When the cavity width is small the disturbance remains confined in the near wall region, whereas when the cavities are large, it extends outward the wall for about 3–4 roughness heights. The peak of u_{rms} for smooth walls occurs at about $y/h = -0.7$. For rough walls it takes place at about $y/h = -1$ (crests plane). This gives an indication that production of the Reynolds stress for smooth and rough wall occurs in different regions.

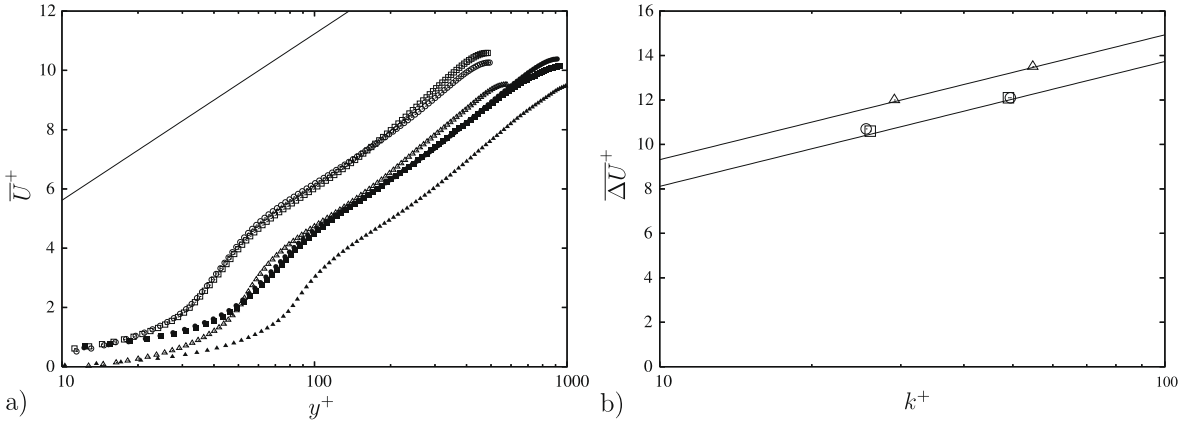

Fig. 6. Velocity profiles in wall units (averages in time, x, z): □, rough-random; ○, rough-modified; △, uniform; ––: $\frac{1}{0.41}\log(y^+)$, empty symbols $Re_b = 2500$, filled $Re_b = 5000$.

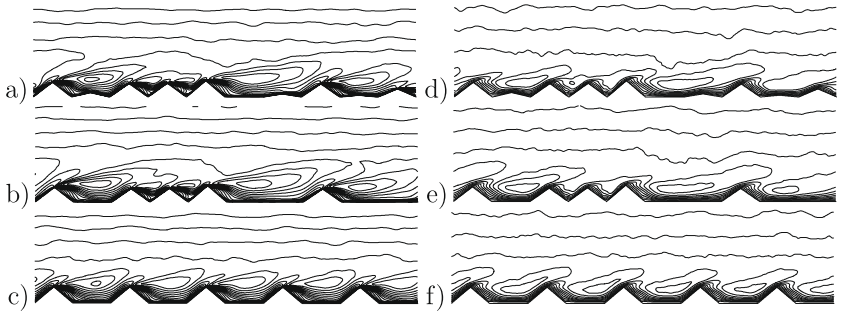

Fig. 7. Contours of streamwise velocity rms (left) and normal-wall velocity rms (right). Increments $\Delta = 0.01$.

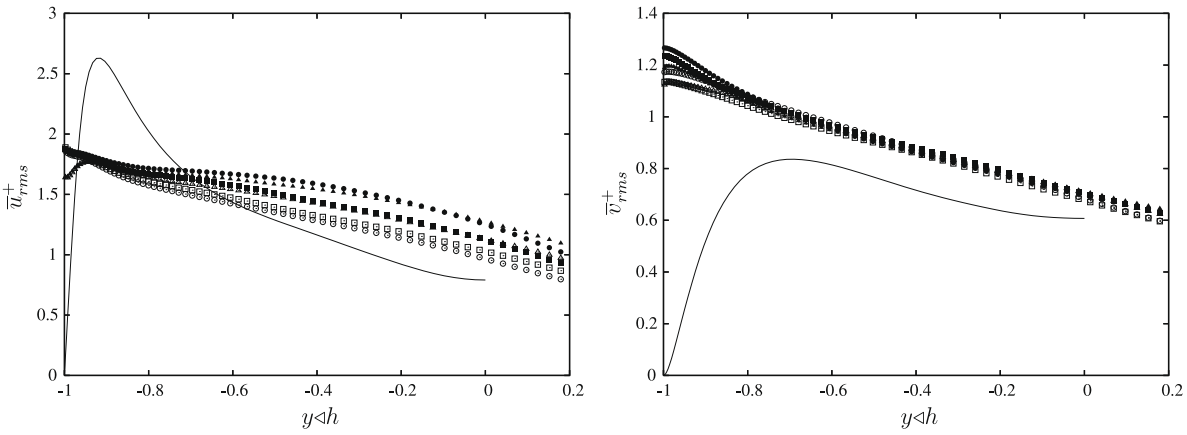

Fig. 8. Streamwise and wall-normal turbulent intensities normalised in wall units: ––, KMMs; □, rough-random; ○, rough-modified; △, uniform; empty symbols $Re_b = 2500$, filled $Re_b = 5000$.

To quantify the overall effect of the roughness surfaces, the rms have been averaged in x, z, t and normalised with the friction velocity (Fig. 8). Even if the streamwise velocity rms increases with respect to a flat wall, when the rms is scaled with the friction velocity, $\bar{u}^+_{rms}$ near the rough wall becomes smaller than that over a flat wall (Fig. 8). The opposite occurs for $\bar{v}^+_{rms}$. Since the ratio u_{rms}/v_{rms} decreases, over a rough wall the flow is more isotropic than over a flat surface. This has been observed by several other experimental and numerical experiments (see Smalley et al. (2002) for a review). Turbulent intensities ($\bar{w}^+_{rms}$ not shown here for sake of brevity) scaled in wall units overlap reasonably well, regardless of the geometrical distribution and of the Reynolds number. Therefore, despite the different spatial distribution, the random, modified and uniform surface present the same overall rms (averages in x, z, t).

The Reynolds shear stress, averaged in x, z, t, scaled with the friction velocity ($\overline{uv}^+_{rms}$), are shown in Fig. 9. The curves overlap closely regardless of Reynolds number and the shape of the surface. With respect to the flat wall, the zero crossing (y_{uv}) of the Reynolds stresses is shifted upward and the slope of the curve is smaller. This is due to different values of the wall shear stress being one wall rough, the other smooth (Leonardi et al., 2005). The maximum value of the Reynolds stress is at the crest plane, as shown also in Fig. 8. While over a flat wall the maximum Reynolds stress represents about 70% of the total stress, here the peak is about 90% of the total stress. Leonardi et al. (2003) showed that uv is correlated

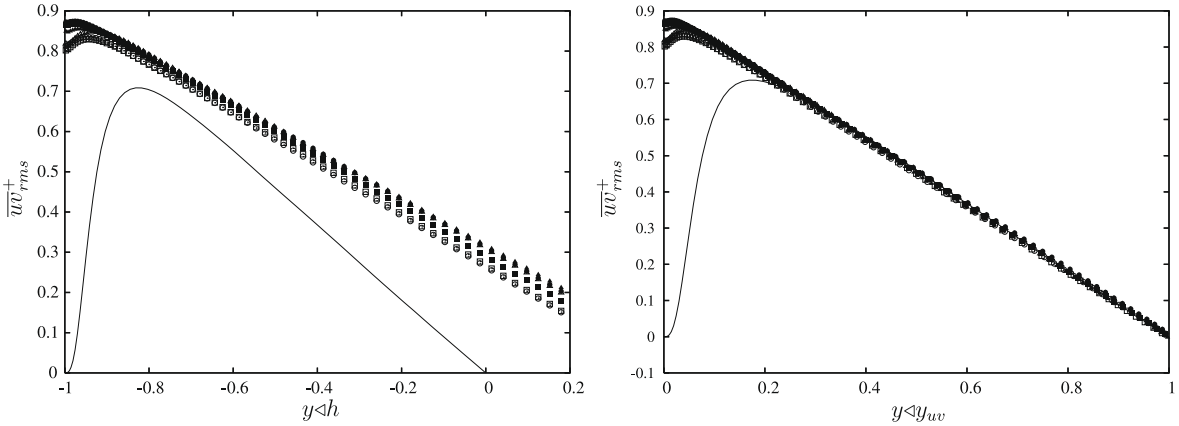

Fig. 9. Reynolds shear stress for the rough and smooth (rough wall side): ——, rough-random; – – –, rough-modified; - - - - rough-uniform; · · · · · ·, smooth. ($\overline{uv}$ means averaged in x, z, t), □, rough-random; ○, rough-modified; △, uniform; empty symbols $Re_b = 2500$, filled $Re_b = 5000$.

with the form drag of the rough surface. Therefore, over a rough wall, the total stress is almost entirely due to the form drag of the surface. This is consistent with recent observations by Brzek et al. (2008) on boundary layers.

Since the present uv profile has a zero crossing (y_{uv}) shifted upward with respect to the centerline, to compare it more effectively with the smooth channel, the wall normal direction has been normalised with y_{uv} (Fig. 9b). The agreement with the smooth wall distribution is remarkable up to $y/y_{uv} = 0.2$ where the profile relative to the smooth wall has a peak and moving towards the wall decreases.

6. Velocity and pressure spectra

To assess how the wall geometry determines the energy distribution among the wavelengths, the energy spectra in the streamwise direction have been calculated. Fig. 10 shows the velocity spectra in the κ_x wave number near the smooth wall, random, modified and uniform rough walls. Near the smooth wall, the spectra of the wall normal velocity is an order of magnitude smaller than the streamwise and spanwise spectra due to the roughness of the wall. Near the rough walls, the spectra relative to the 3 velocity components almost overlap denoting that the flow is more isotropic. The influence of roughness is characterized by energy peaks which mostly occur inside the large eddies scale ($\kappa_x \leqslant L^{-1}$). This implies, that at least near the wall, the roughness affects the large scales. In both the random and modified rough walls the highest peak of the spectra correspond to a wavelength close to the distance between the two higher peaks (5th and 8th). For the modified geometry, the peak of energy is more concentrated near $\lambda = 1.8$. This should be due to the small element between edge 5 and 8 in the random wall which has the

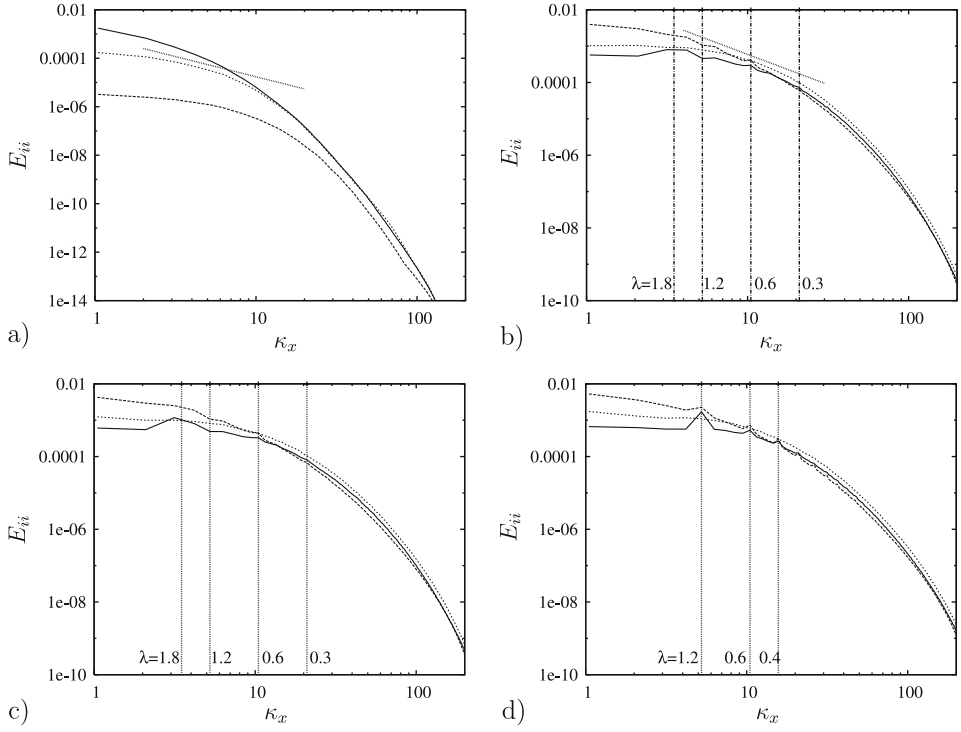

Fig. 10. Velocity spectra in κ_x wave number: ——, normal wall; - - - -, streamwise; ....., spanwise velocities. The straight line has a slope $-5/3$: (a) smooth wall, (b) random, (c) modified, (d) uniform rough wall.

effect of flattening the distribution of energy near the peak. The comparison between the random and modified geometries show a little effect of the smaller elements on the distribution of energy. Overall, the modified geometry represents well the random roughness. For the uniformly-spaced wedges, the highest peak of energy correspond to the distance between two consecutive wedge's peaks ($\lambda = 1.2$). These peak values correspond to the large eddy range and, for the normal direction, can reach values up to 42.7% and 60% higher than for the modified and original-random geometry, respectively. The random and uniform rough wall, despite the different geometries, present both a peak at similar wave numbers.

The spectra of pressure is shown in Fig. 11 near the rough wall, at the centerline and near the upper smooth wall. Near the wall, peaks of energy are observed and corresponds to the distance of the wedges. Moving upward, the energy distribution becomes smoother and the effect of roughness disappears to a close approximation. The energy of pressure is much higher near the rough wall than over the smooth wall. In fact, as shown in the previous sections, roughness increases the pressure drag. In previous studies, Leonardi et al. (2003) showed that the maximum pressure drag and roughness function occur for a pitch to height ratio between 4 and 10. They also showed how the form drag scale with k. Since a random roughness presents ideally all the wavelengths, energy should be maximum for the highest k in correspondence of a $4 < \lambda/k < 10$. Being for the present case $k < 0.2$, the maximum energy should be for $0.8 < \lambda < 2$. This is in fact the range where the maximum energy is observed. The case with uniform elements present similar results to those obtained for the random geometry because its dominant length scale is in the same range.

7. Reynolds stresses budgets

The transport equations for the Reynolds stresses are (Mansour et al., 1988)

$$\frac{Du_iu_j}{Dt} = -\frac{\partial}{\partial x_k}\langle u_iu_ju_k\rangle + \nu\nabla^2\langle u_iu_j\rangle + P_{ij} + \Pi_{ij} - \epsilon_{ij} \tag{4}$$

where $T_{ij} = -\frac{\partial}{\partial x_k}\langle u_iu_ju_k\rangle$ is the turbulent transport term, $D_{ij} = \nu\frac{\partial}{\partial x_k\partial x_k}\langle u_iu_j\rangle$ is the viscous diffusion, $P_{ij} = -\langle u_iu_k\rangle\frac{\partial\langle U_j\rangle}{\partial x_k} - \langle u_ju_k\rangle\frac{\partial\langle U_i\rangle}{\partial x_k}$ is the production term, $\Pi_{ij} = -\frac{1}{\rho}\langle u_i\frac{\partial p'}{\partial x_j} + u_j\frac{\partial p'}{\partial x_i}\rangle$ is the velocity–pressure-gradient tensor and $\epsilon_{ij} = 2\nu\langle\frac{\partial u_i}{\partial x_k}\frac{\partial u_j}{\partial x_k}\rangle$ is the dissipation tensor.

Reynolds stress budgets of $\langle u^2\rangle$ and $\langle v^2\rangle$ are shown in Figs. 12–14, where the transport Eqs. have been non-dimensionalized with u_τ^4/ν. Since the interest is in the overall effects of roughness on the overlying flow, above the roughness sublayer, averages have been done in x, z and t.

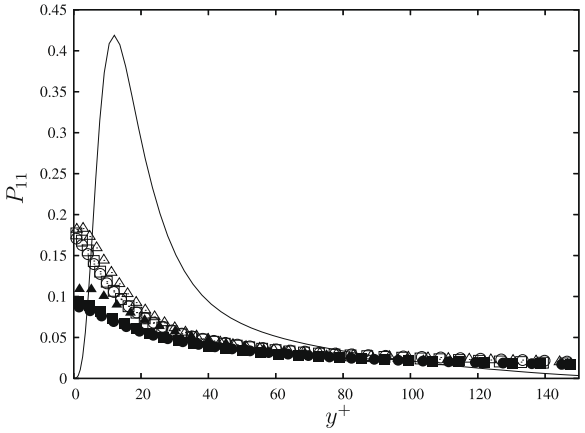

Fig. 12. Production term in the u^2 budget. Lines smooth wall (Mansour et al., 1988), □, rough-random; ○, rough-modified; △, uniform; empty symbols $Re_b = 2500$, filled $Re_b = 5000$.

P_{11} is the dominant production term in the $\langle u^2\rangle$ budget (Fig. 12). Despite the increase of $\langle uv\rangle$, the production term, scaled in wall units decreases with respect to that relative to the smooth wall. In fact, the velocity gradient is much smaller over a rough wall, and the drag is almost entirely due to the pressure drag. More importantly, maximum production of $\langle u^2\rangle$, for a smooth wall, occurs at about $y^+ = 12$ while for the rough surfaces it takes place on the crests plane. The curves relative to the 3 surfaces considered (random, modified, uniform) overlap to a good approximation. Near the crest plane, a Reynolds number effect can be observed. By increasing the Reynolds number, the production, in wall units, decreases. The form drag and as a consequence $\langle uv\rangle$ and P_{11} are little dependent on the Reynolds number. The value of u_τ^4/ν increases with the Reynolds number (u_τ being independent of Re). Therefore, the decrease of the production (when scaled in wall units) with the Reynolds number is due to an increase of the scale u_τ^4/ν.

The main sink in the $\langle u^2\rangle$ budget, in most of the channel, is the velocity–pressure gradient term (Fig. 13b). The non-slip condition at the crests plane applies in a very small portion of the domain, and then the velocity gradients and ϵ_{11} are reduced (note that the smooth wall distribution of ϵ_{11} has been cut to allow the same scale on the vertical axis on both figures). In fact, only near the crest plane the dissipation ϵ_{11} overcomes Π_{11}.

The velocity–pressure correlation redistributes energy from the streamwise component to the spanwise and normal-wall velocity components. In fact Π_{22} is the production term in the budget of

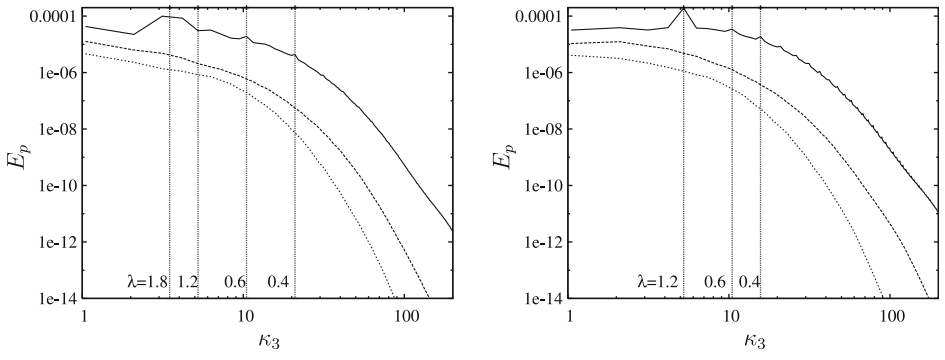

Fig. 11. Pressure spectra as a function of κ_3 (eddies size) and the distance, y, to the rough wall ($\lambda = 2\pi/\kappa_3$): ——, $y = -0.96$; - - - -, $y = 0$;....., $y = 0.975$.

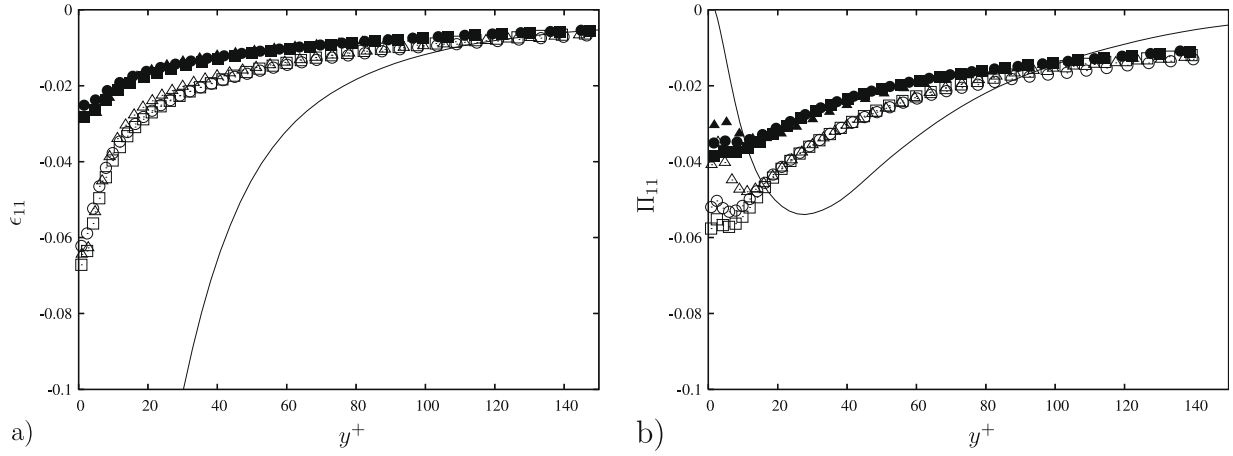

Fig. 13. Dissipation (left) and pressure velocity correlation (right) in the u^2 budget. Lines smooth wall (Mansour et al., 1988), □, rough-random; ∘, rough-modified; △, uniform; empty symbols $Re_b = 2500$, filled $Re_b = 5000$.

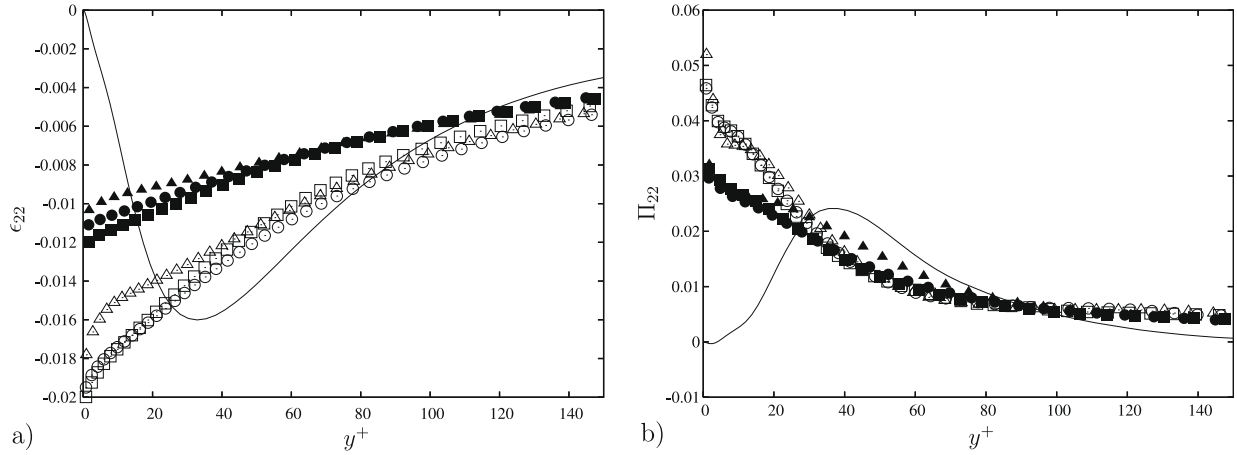

Fig. 14. Dissipation (left) and pressure velocity correlation (right) in the u^2 budget. Lines smooth wall (Mansour et al., 1988): □, rough-random; ∘, rough-modified; △, uniform; empty symbols $Re_b = 2500$, filled $Re_b = 5000$.

$\langle v^2 \rangle$ (Fig. 14b). Far from the wall, Π_{22} resembles that over a flat surface. Near the wall Π_{22} has a maximum while that relative to the smooth surface goes to zero. The excess of energy transferred from $\langle uu \rangle$ to $\langle vv \rangle$ is dissipated near the wall. In fact, for $y^+ < 15$, ϵ_{22} is larger than that relative to the smooth wall (the latter being zero on the wall).

To summarize, over a rough wall, pressure is more effective in extracting energy from the streamwise component and redistributing it to the other stresses, thus improving isotropy. Geroge and Castillo (1997) showed that this is one of the important roles of the pressure–strain rate terms. The turbulent transport terms T_{22} as T_{11} have opposite sign with respect to that over the smooth wall. Energy is therefore transported upward where it is dissipated.

In general, the qualitative behavior of the budgets of u^2 and v^2 is the same over the three different surfaces (random, modified, and uniform). The turbulent transport term T_{22} as T_{11} has the opposite sign than that over the smooth wall. Energy is therefore transported upward where it is dissipated.

8. Conclusions

A DNS for a turbulent channel flow with a 2D random roughness on the lower wall has been performed. The roughness elements are 2D wedges of random height. The roughness geometry has been modified removing the small wedges. Also, a rough profile composed of uniformly-spaced wedges with the same longitudinal area as the random case has been considered for comparison.

It was shown that roughness on the wall induces separated regions, the reattachment occurring on the walls of the wedges or on the bottom walls. The stagnation pressure on the walls of the wedges determine a form drag which is much larger than the viscous drag.

Moreover, the pressure gradients on the walls increase the ejections and inrushes towards the wall. As a consequence the flow is more isotropic. The mechanism inducing to an improved isotropy has been explained in the paper through the Reynolds stress budgets. The pressure redistributes energy between $\langle u^2 \rangle$ and $\langle v^2 \rangle$. As a consequence $\langle v^2 \rangle$ and $\langle w^2 \rangle$ increase and isotropy is better approximated on the rough walls.

Near the wall, the energy spectra presents peaks in correspondence of the pitch over height ratio of the wedges. For the random geometry, the peaks of energy occurs at low wave numbers (i.e. large scales) corresponding to pitch over height ratios in the range $4 < \lambda/k < 10$. Other pitch to height ratio do not affect significantly the energy distribution. As a consequence a random distribution of elements can be simplified by considering only those having a pitch over height in the range $4 < \lambda/k < 10$.

Near the wall, the uniformly distributed roughness represents only a poor approximation of the surface with wedges of random height. The Reynolds stresses, pressure distribution and spectra on the modified wall agree well with those on the random

surface. Far from the wall, all the surfaces have similar results. Therefore, if one is interested in the behavior far from the wall, the average density of the edges can be taken as first approximation. However, if the interest is in the near wall region, or within the roughness layer, only the "modified" wall represents a close approximation of the real rough surface. By removing the small elements on the wake of the larger the overlying flow is not much affected. The geometrical characterization of a rough wall can be simplified to the pitch to height ratio of the largest elements.

Acknowledgement

Caspur is acknowledged for providing computational time, Dr. Amati for his valuable help with the parallel code optimization.

References

Brzek, B., Cal, R.B., Johansson, G., Castillo, L., 2007. Inner and outer scalings in rough surface zero pressure gradient turbulent boundary layers. Physics of Fluids 19, 065101.

Brzek, B., Cal, R.B., Johansson, G., Castillo, L., 2008. Transitionally rough zero pressure gradient turbulent boundary layers. Experiment in Fluids 44, 115–124.

Cheng, H., Castro, I.P., 2002. Near wall flow over urban-like roughness. Boundary-Layer Meteorology 104 (2), 229–259.

Clauser, F.H., 1954. Turbulent boundary layers in adverse pressure gradients. Journal of Aerosol Science 21, 91–109.

Fadlun, E.A., Verzicco, R., Orlandi, P., Mohd-Yusof, J., 2000. Combined immersed boundary finite-difference methods for three-dimensional complex flow simulations. Journal of Computational Physics 161, 35–60.

Flack, K.A., Schultz, M.P., Shapiro, T.A., 2005. Experimental support for Townsend's Reynolds number similarity hypothesis on rough walls. Physics of Fluids 17 (3), 035102:1–035102:9.

Geroge, W.K., Castillo, L., 1997. Zero-pressure-gradient turbulent boundary layer. Applied Mechanics Reviews, 1997.

Ikeda, T., Durbin, P.A., 2007. Direct simulation of a rough-wall channel flow. Journal of Fluid Mechanics 571, 235–263.

Kim, J., Moin, P., Moser, R., 1987. Turbulence statistics in fully developed channel flow at low Reynolds number. Journal of Fluid Mechanics 177, 133–166.

Krogstad, P.A., Andersson, H.I., Bakken, O.M., Ashrafian, A., 2005. An experimental and numerical study of channel flow with rough walls. Journal of Fluid Mechanics 530, 327–352.

Le, H., Moin, P., Kim, J., 1997. Direct numerical simulation of turbulent flow over a backward-facing step. Journal of Fluid Mechanics 330, 349–374.

Leonardi, S., Orlandi, P., Smalley, R.J., Djenidi, L., Antonia, R.A., 2003. Direct numerical simulations of turbulent channel flow with transverse square bars. Journal of Fluid Mechanics 491, 229–238.

Leonardi, S., Orlandi, P., Antonia, R.A., 2005. A method for determining the frictional velocity in a turbulent channel flow with roughness on the bottom wall. Experiment in Fluids 38, 796–800.

Liu, C.K., Kline, S.J., Johnston, J.P., 1966. An experimental study of turbulent boundary layers on rough walls. Rep. MD-15, Department of Mechanical Engineering, Stanford University.

Mansour, N.N., Kim, J., Moin, P., 1988. Reynolds-stress and dissipation-rate budgets in a turbulent channel flow. Journal of Fluid Mechanics 194, 15–44.

McKeon, B.J., Li, J., Jiang, W., Morrison, J.F., Smits, A.J., 2004. Further observations on the mean velocity distribution in fully developed pipe flow. Journal of Fluid Mechanics 501, 135–147.

Nikuradse, J., 1933. Forschungshelft, No. 361, Translated NACA TM 1292..

Orlandi, P., 2000. Fluid Flow Phenomena: A Numerical Toolkit. Kluwer, Dordrecht.

Orlandi, P., Leonardi, S., 2006. DNS of turbulent channel flows with two- and three-dimensional roughness. Journal of Turbulence 7 (53).

Perry, A.E., Schofield, W.H., Joubert, P.N., 1969. Rough wall turbulent boundary layers. Journal of Fluid Mechanics 37, 383–413.

Rotta, J.C., 1962. Turbulent boundary layer incompressible flow. Progress in Aeronautical Sciences, vol. 2. Pergamon press, Oxford.

Schlichting, H., 1960. Boundary Layer Theory. McGraw–Hill, New York.

Smalley, R.J., Leonardi, S., Antonia, R.A., Djenidi, L., Orlandi, P., 2002. Reynolds stress anisotropy of turbulent rough wall layers. Experiment in Fluids 33, 31–37.

Shockling, M.A., Allen, J.J., Smits, A.J., 2006. Roughness effects on turbulent pipe flow. Journal of Fluid Mechanics 564, 267–285.

Schultz, M.P., Flack, K.A., 2005. Outer layer similarity in fully rough turbulent boundary layers. Experiments in Fluids 38, 328–340.